

Thermal Neutron Backscatter Imaging

Peter Vanier

*Presented at the 2004 IEEE NNS/MIC/SNPS and RTSD Conference
Rome, Italy
October 16-22, 2004*

October 2004

**Nonproliferation and National Security Department
Detector Development and Testing Division**

Brookhaven National Laboratory

P.O. Box 5000
Upton, NY 11973-5000
www.bnl.gov

Managed by
Brookhaven Science Associates, LLC
for the United States Department of Energy under
Contract No. DE-AC02-98CH10886

DISCLAIMER

This report was prepared as an account of work sponsored by an agency of the United States Government. Neither the United States Government nor any agency thereof, nor any of their employees, nor any of their contractors, subcontractors, or their employees, makes any warranty, express or implied, or assumes any legal liability or responsibility for the accuracy, completeness, or any third party's use or the results of such use of any information, apparatus, product, or process disclosed, or represents that its use would not infringe privately owned rights. Reference herein to any specific commercial product, process, or service by trade name, trademark, manufacturer, or otherwise, does not necessarily constitute or imply its endorsement, recommendation, or favoring by the United States Government or any agency thereof or its contractors or subcontractors. The views and opinions of authors expressed herein do not necessarily state or reflect those of the United States Government or any agency thereof.

Thermal Neutron Backscatter Imaging

Peter E. Vanier, Leon Forman, Stephen J. Hunter, Emma J. Harris, and Graham C. Smith, Member, IEEE

Abstract-- Objects of various shapes, with some appreciable hydrogen content, were exposed to fast neutrons from a pulsed D-T generator, resulting in a partially-moderated spectrum of backscattered neutrons. The thermal component of the backscatter was used to form images of the objects by means of a coded aperture thermal neutron imaging system. Timing signals from the neutron generator were used to gate the detection system so as to record only events consistent with thermal neutrons traveling the distance between the target and the detector. It was shown that this time-of-flight method provided a significant improvement in image contrast compared to counting all events detected by the position-sensitive ^3He proportional chamber used in the imager. The technique may have application in the detection and shape-determination of land mines, particularly non-metallic types.

I. INTRODUCTION

THE detection of land mines and other hidden explosives requires new technologies for reducing false positive signals and increasing sensitivity to non-metals [1]. We have begun trial measurements to evaluate a technique in which thermal neutron backscatter imaging (TNBI) could be used in both detection and shape determination of explosives. Depending on the outcome of such evaluations and subsequent improvements in the design of prototypes, this technique could have future applications in countering terrorism and in preventing proliferation of weapons of mass destruction. The technique relies on the ability of low-Z dense materials (which includes explosives) to moderate and thermalize incident fast neutrons. Using a suitable pulsed neutron source and imager, our goal is to develop a system that has improved penetrability and better diagnostic imaging capability over existing methods. The system utilizes a commercial high-energy neutron generator and a two-dimensional ^3He proportional chamber, together with a coded aperture mask. This effort

Manuscript received October 14, 2004. This work was supported in part by the U.S. Department of Energy under Contract No. DE-AC02-98CH10886.

P. E. Vanier is with the Nonproliferation and National Security Department, Brookhaven National Laboratory, Upton, NY 11973, USA (telephone: 631-344-3535, e-mail: vanier@bnl.gov).

L. Forman is a consultant with the Nonproliferation and National Security Department, Brookhaven National Laboratory, Upton, NY 11973, USA (telephone: 631-344-5852, e-mail: lforman@bnl.gov).

S. J. Hunter is with Defence Science and Technology Laboratory, Ft. Halstead, Sevenoaks, Kent TN14 7BP, UK (telephone: 44 1959 892887, e-mail: sjhunter1@mail.dstl.gov.uk).

E. J. Harris is with Defence Science and Technology Laboratory, Ft. Halstead, Sevenoaks, Kent TN14 7BP, UK (telephone: 44 1959 892971, e-mail: ejharris@mail.dstl.gov.uk).

G. C. Smith is with the Instrumentation Division, Brookhaven National Laboratory, Upton, NY, USA (telephone: 631-344-4253, e-mail: gsmith@bnl.gov).

represents a further development of neutron imaging with coded apertures [2]-[4] using high-resolution position-sensitive neutron detectors with very good long-term position stability [5].

II. EXPERIMENTAL DETAILS

The major components of the thermal neutron imager are shown in Fig. 1. The basis of this instrument is a 2-dimensional 20 cm x 17 cm position-sensitive proportional counter (1) containing about 6 atmospheres of ^3He . A thermal neutron reacts with ^3He to form a proton and a triton with total kinetic energy of 764 keV that is available to ionize electrons in the gas. In the proportional mode, the applied bias field is sufficient to cause some electron multiplication. The motion of the electrons and positive ions in the bias field induces positive charges on the two perpendicular, planar arrays of cathode wires, or strips, with 1.6-mm spacing. These wires (strips) are connected to charge-sensitive preamplifiers at resistively coupled nodes spaced at 1-cm intervals. The center of charge in x and y dimensions is determined to within about 1 mm by resistive charge division between the three preamplifier nodes closest to the event. The location of the event in the z direction (perpendicular to the face of the detector) has an uncertainty d less than the 1.5-cm thickness of the gas and should be approximately equal to the mean free path of thermal neutrons in the ^3He . This uncertainty can lead to a parallax error in the decoding of x and y positions if the incident neutron path is not perpendicular to the face.

All of the position-encoding electronics required to create a digital histogram are now contained in a single custom board (2). The histogram can be initialized or interrogated, when required, by a computer (3) that performs further analysis of the data. Shadows are cast on the front of the detector by a coded aperture constructed from Cd sheet glued to an Al substrate. The three mask patterns in use at BNL are Modified Uniformly Redundant Arrays [6], with 19, 31 or 47 pixels on a side (see Fig. 2). These patterns are antisymmetric, and so will replace open areas with closed areas when they are rotated by 90 degrees. The other 5 sides of the detector are shielded from scattered neutrons by a Cd-lined box equipped with 4 support frames on which the mask can be clipped at different distances from the face of the detector so as to change the focal length, f .

When the coded aperture camera is used to image nearby objects, the basic mask pattern must be fabricated with dimensions smaller than the sensitive area of the detector, so that the magnified shadow of the primitive mask pattern is entirely recorded (see Fig. 3). Four copies of the basic pattern are tiled together so that a complete mask shadow can be cast from a point source that is off the central axis. For an $n \times n$ -pixel mask pattern with pixel size p , the width s of the scene at a range r that is fully encoded is given by

$$s = np(1 + r/f) \quad (1)$$

Sources to be imaged should be kept within this field of view or they may contribute to partially encoded data, which will introduce artifacts into the images. The spatial resolution of the imager is limited by p for distant sources, and becomes worse for nearby sources because of the magnification of the pixel shadow and the uncertainty in the z location of the neutron interaction in the ^3He .

These effects are described parametrically in Fig. 4 where the shadow of a pixel on the face of the detector is kept constant by adjusting the mask pixel size as a function of source distance. The parallax error is given by dh/r . For a very distant object (large r), the shadow of a pixel approaches the same size as the mask pixel p , and there is negligible parallax error, but the actual size of an object, rp/f , that matches one resolution element becomes large. For a source closer than 100 cm, the parallax error approaches the dimensions of a pixel shadow, so the image becomes blurred. With the given choice of mask dimensions and focal length, it is difficult to resolve objects smaller than 1 cm.

III. TESTS OF THE IMAGER

Preliminary measurements have been made of the imaging capability of the system using a continuous isotopic source. An Am/Be source has been enclosed by 30-cm thick moderating material and surrounded by boron-loaded polyethylene shielding, leaving an aperture about 15 cm in diameter from which thermal neutrons emanate. A photo of this circular aperture is shown in Fig. 5, with a triangular block of wood with thickness 3.75 cm interposed in the neutron pathway. The neutron detector and coded aperture mask were placed about 1 m away.

The deconvolved thermal neutron image is shown in Fig. 6, and it is very clear that the system has successfully identified the circular source of neutrons with a deficit of neutrons at the position of the wooden triangle. A major fraction of the thermal neutrons incident on the back of the wooden triangle were scattered in other directions so they were not collected by the imager. A much smaller number of neutrons that were initially traveling at oblique angles were scattered back into the field of view. The net result was a triangular shadow that was

dark compared to the intensity of thermal neutrons leaving the surface of the polyethylene cylinder.

IV. TIME-OF-FLIGHT MEASUREMENTS

A commercial D-T pulsed neutron generator was used to produce 10^7 fast neutrons per second (14 MeV) in pulses having a 1 kHz repetition frequency. Objects containing hydrogen placed in the fast neutron beam then thermalized some fraction of the neutrons, and became secondary sources. A crucial issue in producing useful images with a neutron generator is the ability to veto events that do not contribute to the image. Fig. 7 shows the calculated neutron current as a function of flight time from a hydrogenous target to the detector, for three different distances of separation, 1, 2 and 3 meters. It is assumed that the neutrons in each bunch achieve a Maxwellian distribution of energies corresponding to a temperature of 25 meV before they are emitted from the target.

In addition, epithermal neutrons that arrive at the detector at times shorter than 100 μs can penetrate the cadmium mask and have a finite probability of being detected by the ^3He without casting a shadow. Also, neutrons that thermalize in the floor and walls arrive at the detector from all directions at later times. These events add a uniform fog to the image. Many of them can be rejected by gating the acquisition system to accept only those events detected during the period 100 to 500 μs after the neutron generator pulse. Thus the gated image emphasizes thermal neutrons with the appropriate time-of-flight for the target to camera range of 1 m.

Fig. 8 shows experimental data in which the time-of-flight gate was varied both with and without a thermalizing target in the field of view. The high count rate at early time is due to the detector response to fast and epithermal neutrons where the presence of the target makes little difference to the detected count rate and the thin cadmium coded aperture elements are not effective for stopping the neutrons. The ^3He reaction cross-section for fast neutrons may be perhaps 1000 times less than for thermal neutrons, and the detector response to 1 eV neutrons is about 10 times less than at thermal energies. However, the number of scattered fast neutrons is relatively high. The physical principles of fast neutron emission from bulk media are termed die-away and are quite complex. The time of emission of neutrons of any given energy first requires a slowing down time to that energy and then a leakage time at that energy. It is important to note that the addition of the small target (1% of the area of the scene) increased the total count rate at longer time delays by a factor of about 2.

In order to determine the relative contrast that might be obtained from this neutron energy spectrum with cadmium (Cd) or 5% borated polyethylene (BPE) sheet used separately or together in a coded aperture, four quadrants were shielded as shown in Fig. 9. The Cd shields the thermal neutrons

effectively, while the BPE absorbs some of the fast and epithermal neutrons.

The results of the contrast test were, as expected, dependent on the timing gate used to select the collected neutrons. In the ungated case (Fig. 10), the best contrast ratio obtained was about a factor of 2 between the unshielded area and the area shielded with Cd, indicating a significant contribution from epithermal neutrons that penetrated the Cd. When the 100-500 microsecond gate was employed (Fig. 11), a contrast ratio of 6 was achieved. Although the ungated data show a higher net thermal neutron count per pixel, many of these neutrons could be from room background rather than from the target at 1 m range, and would be distributed throughout an image.

Figure 12 shows images acquired using a cylindrical polyethylene target 10 cm in diameter x 10 cm long with the axis of the cylinder facing the imager, and perpendicular to the neutron beam coming from below. The image formed with ungated events (a) contained 149,000 counts, of which half should be thermal. This image did not distinguish the target from the background that included thermal neutrons from the walls and ceiling. The gated image (b) contained 98,000 counts, of which 80% should be thermal. This image clearly showed the circular face of the cylinder at the center of the image, with a diameter equal to about 3 mask pixels. The timing gate of 150-600 microseconds was chosen, based on the calculations in Fig. 7, to optimize the sensitivity to a target at approximately 1 m from the detector.

Figure 13 shows a photo of a more complex shape constructed from square sheets of polyethylene underneath a large paraffin wax candle clamped at an angle. The fast neutrons traveled vertically from the shielded box below this target assembly, and illuminated the full length of the underside of the candle. The neutron image, shown in Fig. 14, which included 10^6 counts, shows the plates and the candle quite clearly.

V. CONCLUSIONS

Thermal neutron backscatter imaging of hydrocarbon materials has been demonstrated using a D-T 14-MeV neutron generator and a coded aperture camera. Gating of the acquisition system to emphasize the thermal neutrons that travel a known distance from a target zone is one way to enhance the quality of the images. The shapes of hydrogenous objects can be determined by this technique, provided enough events are recorded to obtain statistically significant intensities in the regions of interest. Future work will include the merging of mask and anti-mask data to reduce artifacts in the images caused by mask and detector imperfections. The construction of larger, more sensitive detectors would significantly reduce the data acquisition time.

VI. ACKNOWLEDGEMENTS

The authors are grateful to Dr. Lucian Wielopolski and Dr. Sudeep Mitra for the loan of the neutron generator and for their assistance in performing the neutron thermalization and time-of-flight experiments. Neil Schaknowski and Joe Mead were extremely helpful in preparing the ^3He detector and the data acquisition system for these experiments.

VII. REFERENCES

- [1] C.P. Datema, V.R. Bom, C.W.E. van Eijk, "Monte Carlo simulations of landmine detection using neutron backscattering imaging", *Nucl. Instrum. & Meth.* vol. A513, pp. 398-402, 2003
- [2] P. E. Vanier, and L. Forman, "Advances in Imaging with Thermal Neutrons", *Proceedings of the Institute of Nuclear Materials Management, 37th Annual Meeting, Naples, FL, July, 1996.*
- [3] P.E. Vanier and L. Forman, "Forming images with thermal neutrons", *SPIE International Symposium on Optical Science and Technology, Conference vol. 4784A, Hard X-rays, Gamma Rays and Particles, Seattle, WA, July, 2002.*
- [4] P.E. Vanier, "Improvements in coded aperture thermal neutron imaging", *SPIE International Symposium on Optical Science and Technology, Conference vol. 5199A, Penetrating Radiation Systems and Applications, San Diego, CA, August, 2003.*
- [5] B. Yu, J.A. Harder, J.A. Mead, V. Radeka, N.A. Schaknowski and G.C. Smith, "Neutron Detector Development at Brookhaven", *Nucl. Instrum. & Meth.* vol. A513, pp. 362-366, 2003.
- [6] G. S.R. Gottesman and E.E. Fenimore, "New family of binary arrays for coded aperture imaging", *Applied Optics*, vol. 28, pp. 4344-52, 1989.

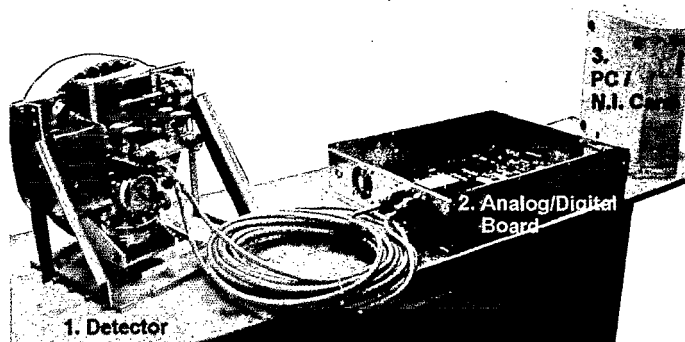


Fig. 1. Components of thermal neutron coded aperture imager.

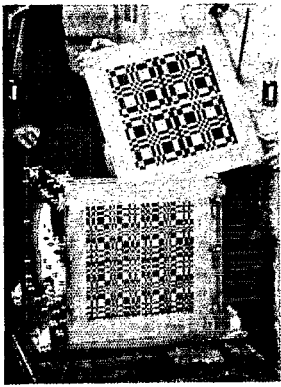


Fig. 2. Cadmium coded aperture and shielded camera box.

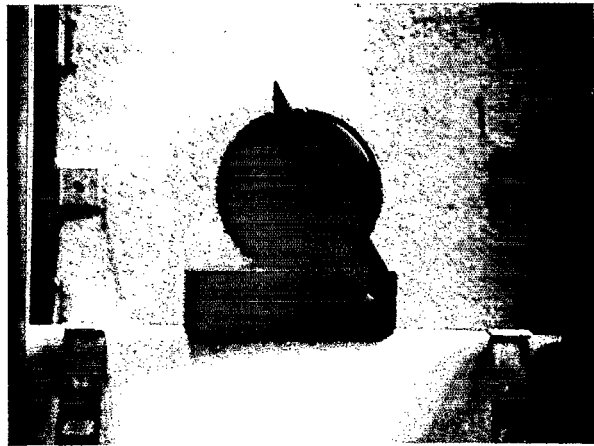


Fig. 5. Photo of circular output aperture of moderated Am/Be neutron source, with triangle of wood interposed in the neutron beam.

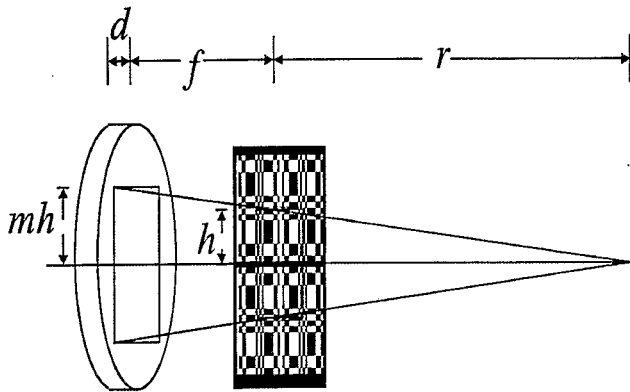


Fig. 3. Geometrical factors that limit resolution of the coded aperture imager.

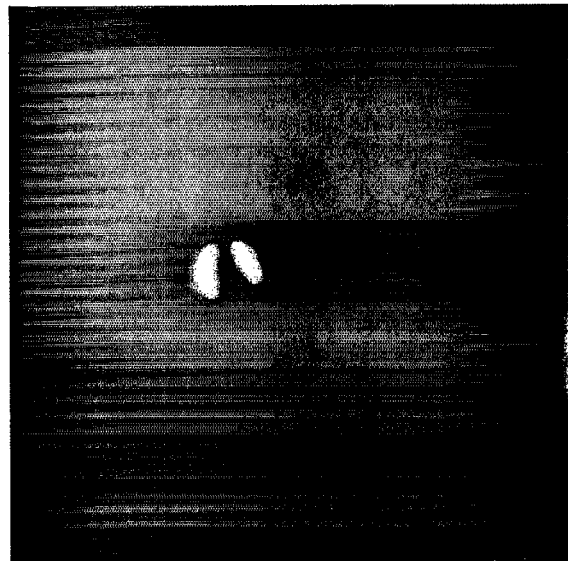


Fig. 6. Thermal neutron image of Am/Be source in Fig. 5. The scale is about half of that for the optical photograph.

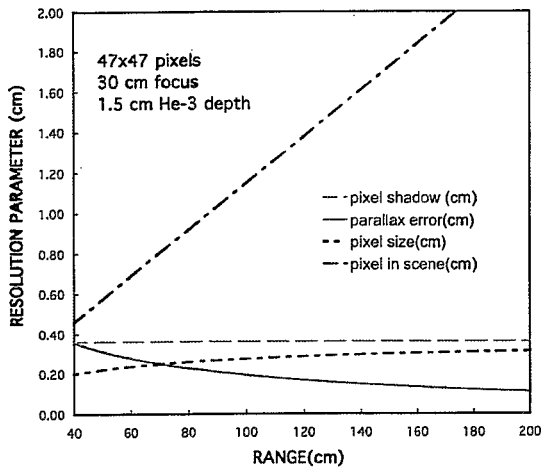


Fig. 4. Spatial resolution is limited by mask pixel size at long range and by parallax in the ^3He at short range. The detector resolution is about 0.1 cm.

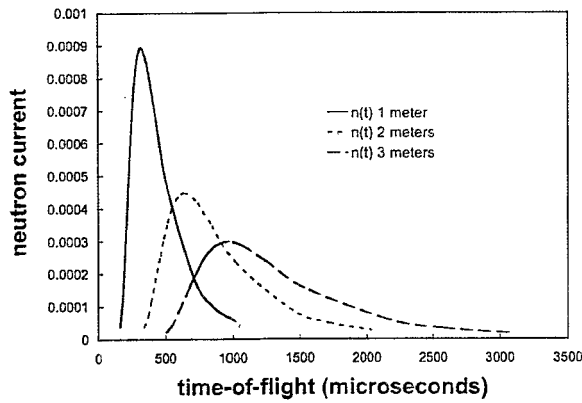


Fig. 7. Relative neutron currents versus time-of-flight for various flight paths between the thermalizing source and detector, for a 25 meV Maxwellian distribution.

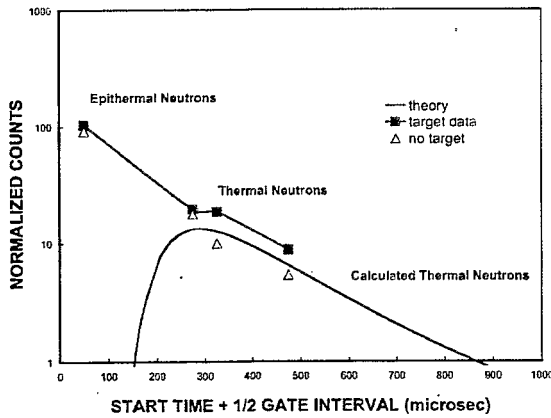


Fig. 8. Total count rate with and without a small target in the field of view.

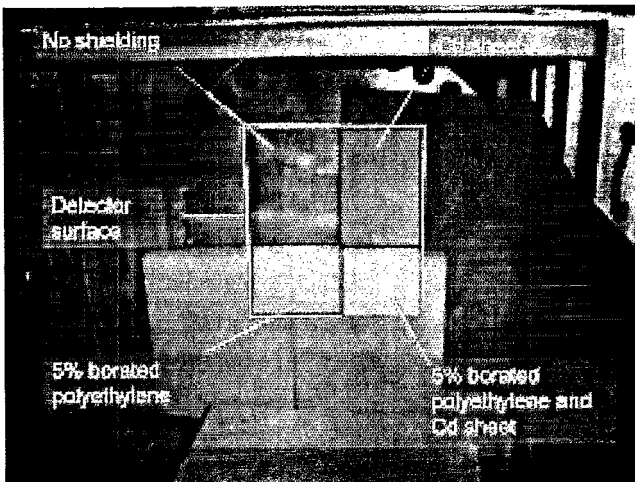


Fig. 9. Test configuration to determine available mask contrast with D-T source and moderator.

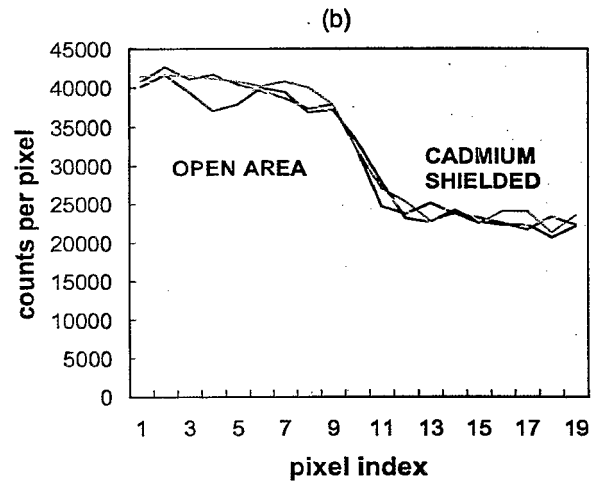
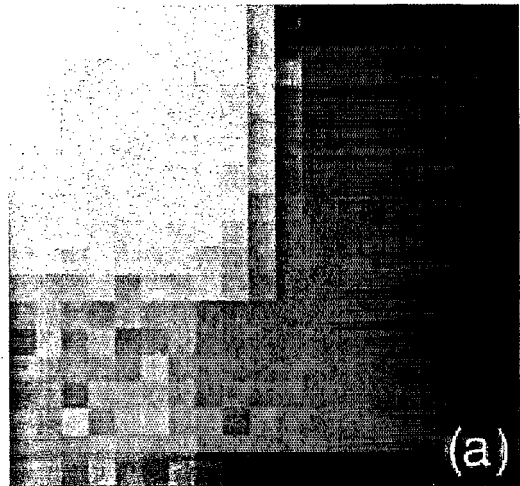
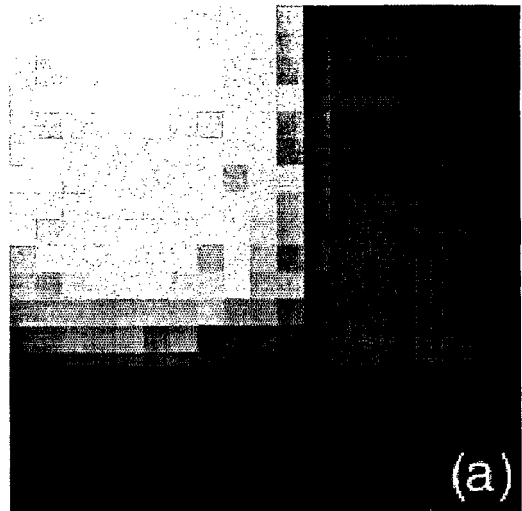


Fig. 10. (a) Shadow cast by shielding in Fig. 9 with no gating, binned to match 19 x 19 mask pixels, and (b) profile of counts in top 4 rows of bins.



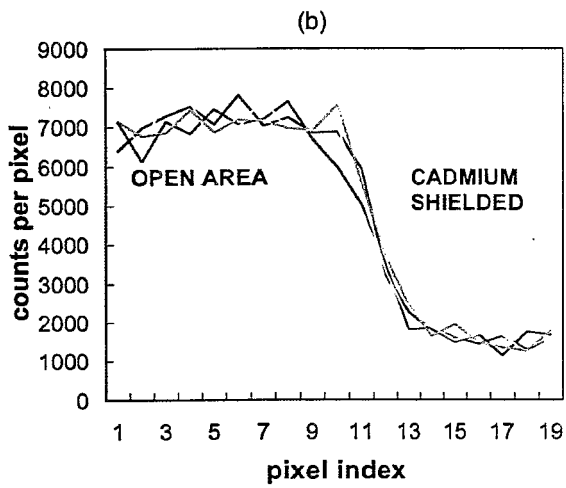


Fig. 11. (a) Shadow cast by shielding in Fig. 9 with gating. binned to match 19 x 19 mask pixels, and (b) profile of counts in top 4 rows of bins.



Fig. 13. Photo of complex shape of thermalizers including square PE plates and large candle tilted towards camera.

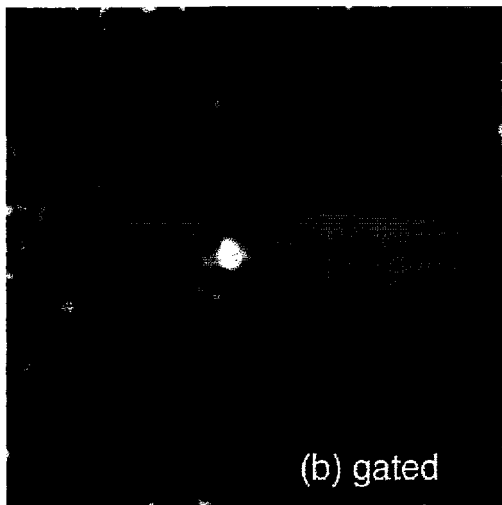
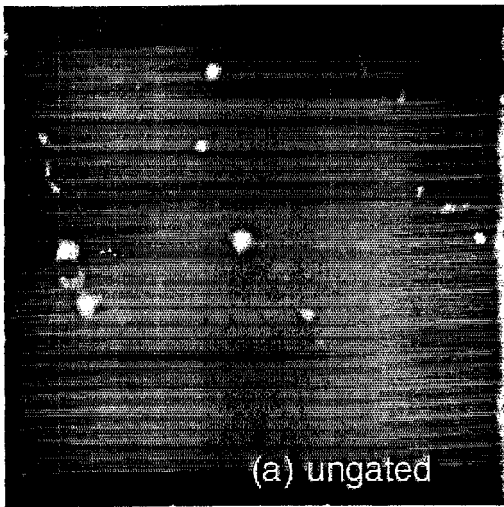


Fig. 12. Images of a PE cylinder obtained with and without gating.

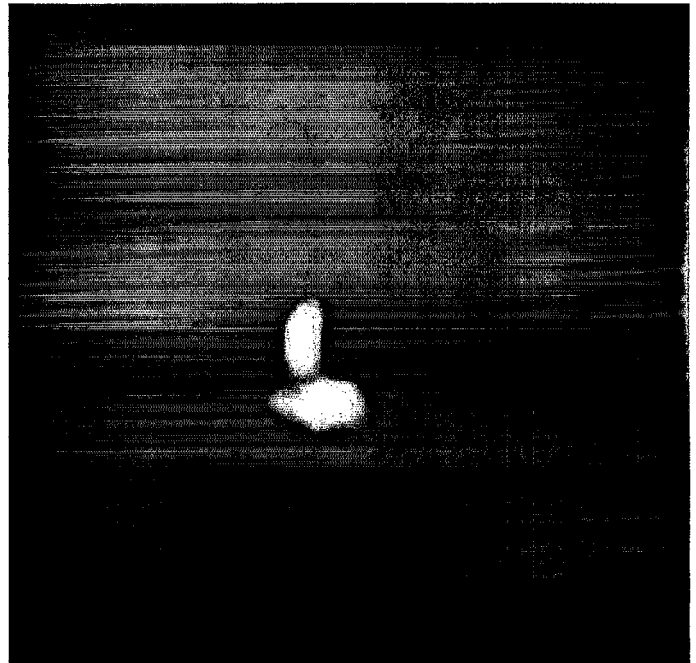


Fig. 14. Thermal neutron image of shape in Fig. 13.